ChemPhysChem

Research Article
doi.org/10.1002/cphc.202200768

Chemistry Europe
European Chemical Societies Publishing

www.chemphyschem.org

Nature and Strength of Weak O···O Interactions in Nitryl Halide Dimers

Andre Nicolai Petelski,*[a] Darío Jorge Roberto Duarte,*[b, c] and Nélida María Peruchena*[b, c]

Dedicated to Professor Gladis Laura Sosa

The use of real space functions and molecular graphs has pushed some chemists to wonder: Are interactions between negatively charged oxygen atoms possible? In this contribution we analyze whether there is a real interaction between oxygen atoms in nitryl halide dimers $(XNO_2)_2$ (X = F, Cl, Br and I) and in tetranitromethane and derivatives. Based on ab-initio and density functional theories (DFT) methods, we show these complexes are weakly stabilized. Energy decomposition analyses based on local molecular orbitals (LMOEDA) and interacting quantum atoms (IQA) reveal both dispersion and exchange play a crucial role in the stabilization of these complexes. Electron charge density and IQA analyses indicate that the oxygen atoms are connected by privileged exchange channels. In addition, electrostatic interactions between O and N atoms are also vital for the stabilization of the complexes. Finally, a reasonable explanation is given for the dynamic behavior of nitryl groups in tetranitromethane and derivatives.

Introduction

The interaction between oxygen atoms (O···O) have been analyzed for many years in a wide variety of systems. Here we must distinguish two types of O···O interactions: intra- and intermolecular ones. One of the first theoretical observations of a bond critical point (BCP) between oxygen atoms was done by Cioslowski et al.[1] in the framework of the Quantum Theory of Atoms in Molecules (QTAIM) of Bader.[2] Later on, Zhurova and co-workers[3] studied an O···O interaction in the dinitramide anion. They concluded that these interactions between negatively charged oxygen atoms can be characterized as bonding closed-shell interactions in the framework of QTAIM. In a theoretical study of neutral molecules like enol forms of cis-β-diketones, Pakiari and Eskandari[4] showed that the 1,8-naphtalenediol (A) is more stable than the 1,5-naphtalenediol (B) by 5.47 kcal/mol at the B3LYP functional and 8.15 kcal/mol within MP2 computations. This difference was attributed to O···O interactions present in compound A. In addition, by employing the QTAIM, these researchers also indicated that the O···O interactions are within the closed-shell regime and delocalization indices between oxygen atoms indicate a small O–O bond order. However, Jabłoński carried out high-level ab initio calculations on X···O (X = F, Cl, Br, I and O) intramolecular interactions and disproved Pakiari's results.[5] Through a deep energetic analysis of conformers, isodesmic reactions, and electrostatic potential maps, Jabłoński concluded that such O···O interactions are repulsive. He also suggested that only negative values of interaction energies should be considered as sufficient evidence of attractive interactions and not the mere appearance of a BCP. In this context, Sharma et al.[6] studied the crystal structures of quinolone carboxylate and biseth-oxycarbonyl-vinylaniline derivates containing the O···O intramolecular interaction through QTAIM and natural bond orbital (NBO) analyses. They found out that the lone pair electrons of oxygens atoms undergo stabilization due to negative hyperconjugation and maintains the otherwise repulsive O···O close contact. In this case, they obtained a negative interaction energy according to an isodesmic reaction. In a similar case, Fellowes et al.[7] also showed experimental evidence on the existence of a short O···O contact between a divalent oxygen and an oxygen of the nitro group within an o-nitro-O-aryl oxime.

With regards to the intermolecular O···O interactions, they were mainly identified within electron densities of crystal structures. For instance, Bianchi et al.[8] found an intermolecular O···O contact (O–O distance shorter than the sum of the van der Waals radii) between $Mn_2(CO)_{10}$ complexes in metallo-carbonyl crystals through an accurate X-ray diffraction analysis at 120 K. Besides, Arumuganathan et al.[9] also reported a close O···O contact between polyoxometalate moieties of cis-$\{MoO_2\}$ complexes. In another QTAIM study on

[a] Dr. A. N. Petelski
Departamento de Ingeniería Química
Grupo de Investigación en Química Teórica y Experimental (QUITEX)
Universidad Tecnológica Nacional, Facultad Regional Resistencia
French 414 (H3500CHJ), Resistencia, Chaco, Argentina
E-mail: npetelski@frre.utn.edu.ar
[b] Dr. D. J. R. Duarte, Prof. Dr. N. M. Peruchena
Laboratorio de Estructura Molecular y Propiedades
Instituto de Química Básica y Aplicada del Nordeste Argentino
IQUIBA-NEA (UNNE-CONICET)
Avenida Libertad 5460 (3400), Corrientes, Argentina
E-mail: djr_duarte@hotmail.com
perunm2014@gmail.com
[c] Dr. D. J. R. Duarte, Prof. Dr. N. M. Peruchena
Departamento de Química,
Facultad de Ciencias Exactas y Naturales y Agrimensura, Universidad Nacional del Nordeste,
Avenida Libertad 5460 (3400), Corrientes, Argentina

Supporting information for this article is available on the WWW under https://doi.org/10.1002/cphc.202200768

the crystal structure of dinitrogen tetroxide, Tsirelson et al.[10] have found that the multiple O···O interactions between N_2O_4 molecules can also be characterized as "hole-lump" interactions. They also stated that the correlation energy plays a key role along the O···O bond paths. There are other crystallographic studies reporting O···O interactions but they only support their findings on a few topological parameters.[11–13] Furthermore, when oxygen is bonded to some electron-withdrawing fragments (like fluorine, in OF_2) it can form an O-centered chalcogen-bonding interaction with several Lewis bases.[14–16] The interaction energy of these type of complexes is originated not only from the primary chalcogen, but also from the contribution of other secondary interactions.

As previously shown, the presence of bond paths and BCPs between two oxygen atoms has encouraged researchers to analyze its nature. In this context, there have been interesting advances about the role of electronic exchange in the mental image of chemical graphs within the last few years. Pendás et al.[17] were the firsts to propose that the bond path of the QTAIM indicates primary exchange channels. That is, an atom is bonded by bond paths with those neighbors with which exchange-correlation component is maximized. Jabłoński rebutted this idea by showing a large set of examples of interactions that violate the concept of privileged exchange channels proposed by Pendás and his co-workers.[18] Recently, Levina et al.[19] have used a set of advanced bonding descriptors to characterize several intermolecular D–H···A hydrogen bonds. In their study of 150 isolated and solvated molecular complexes, they explained how electron exchange defines the bonding picture in the proximity of H···A BCPs.

Despite the existing information on the short O···O contacts it is evident that there is still much research to be done on the nature of these peculiar interactions. To deepen our understanding on this topic, we investigated O···O contacts between XNO_2 nitryl halides (X = H, F, Cl, Br and I) in the gas phase and $[XC(NO_2)_3]_2$ dimers (X = H, Cl, and NO_2) in the gas phase and crystalline structures obtained from the Cambridge Crystallographic Data Centre (CCDC).

Computational Details

Structure and Interaction Energies

All computations were performed with Gaussian 09.[20] All nitryl halides (XNO_2, X = H, F, Cl, Br and I) and their corresponding dimers were fully optimized using the Møler-Plesset second-order (MP2) perturbation theory[21] with the aug-cc-pVTZ basis set. For the iodine atom the aug-cc-pVTZ-PP basis set was used.[22] Tetranitromethane and derivatives were fully optimized at M062X/6-311++G(2d,2p) level. All complexes were verified as true minima by a vibrational frequency analysis. Single point computations were also performed at the Hartree-fock (HF) and the Coupled Cluster single-double and perturbative triple [CCSD(T)] levels of theory. Complete Basis Set (CBS) extrapolation scheme has been applied using the proposal of Halkier et al.[23,24] following the recommendations of Hobza et al.[25] All interaction energies were computed with Equation (1) as the difference between the energy of the dimer E_{AB} and the energy of the monomers E_A and E_B with the structure they acquire in the complex AB (indicated by the superscripts). Considering there are various reports that have indicated that the uncorrected interaction energy with large basis sets provides a better estimate than the Counterpoise method, the basis set superposition error (BSSE) was not computed.[26]

$$\Delta E_{int} = E_{AB} - E_A^{AB} - E_B^{AB} \quad (1)$$

Energy Decomposition Analyses

It is a well-known fact that the different existing methods for energy decomposition analysis (EDA) can lead to contradictory interpretations.[27,28] To analyze the energetic components that predominate in the stabilization of these complexes, we have carried out the EDA with two methodologies that perform the decomposition using very different algorithms. The local molecular orbital energy decomposition analysis[29] (LMOEDA) method is derived from the Kitaura and Morokuma decomposition scheme,[30] while the IQA[31] method is derived from the QTAIM.[2]

In the LMOEDA scheme,[29] the interaction energy is partitioned according to Equation (2):

$$\Delta E_i(\mathrm{LMOEDA}) = \Delta E_{el} + \Delta E_{ex} + \Delta E_{rep} + \Delta E_{pol} + \Delta E_{disp} \quad (2)$$

where ΔE_{el} is the electrostatic component, ΔE_{ex} is the attractive exchange component and ΔE_{rep} is the repulsive term, both resulting from the Pauli exclusion principle, ΔE_{pol} and ΔE_{disp} correspond to polarization and dispersion terms, respectively. LMOEDA calculations were carried out using the GAMESS[32] quantum chemistry package.

The IQA scheme is a very useful tool to characterize the nature of the molecular interactions. The interaction energies, E_{int}(IQA) [Eq. (3)], can be decomposed in three contributions: deformation (E_{def}), classic (E_{cl}) and quantum (E_{xc}) terms.

$$E_{int}(\mathrm{IQA}) = E_{def} + E_{cl} + E_{xc} \quad (3)$$

IQA method can also calculate the energies of the interatomic interactions. These energies can be split up into five terms [Eq. (4)].

$$E_{int}(A,B) = V_{nn}(A,B) + V_{en}(A,B) + V_{ne}(A,B) + V_{ee,C}(A,B) + V_{ee,xc}(A,B) \quad (4)$$

Where E_{int}(A,B) is the interatomic interaction energy, V_{nn}(A,B) is the repulsion energy between nuclear charge of atom A and nuclear charge of atom B, V_{en}(A,B) is the attraction energy between nuclear charge of atom B and electron density distribution of atom A, V_{ne}(A,B) is the attraction energy between nuclear charge of atom A and electron density distribution of atom B, $V_{ee,C}$(A,B) is the Coulomb part of two-electron interaction energy between atom A and atom B, $V_{ee,xc}$(A,B) is the exchange-correlation part of two-electron interaction energy between atom A and atom B. The first four terms correspond to Coulombic interactions [E_{cl}(A,B)] and the last term is exchange-correlation contribution [E_{xc}(A,B)]. Therefore, the interatomic interaction energies [Eq. (5)] can be written as:

$$E_{int}(A,B) = E_{cl}(A,B) + E_{xc}(A,B) \quad (5)$$

IQA calculations have been performed with AIMAll[33] program.

Electron Charge Density Analyses

The intermolecular distribution of the electronic charge density $\rho(\mathbf{r})$ was analyzed within the framework of the QTAIM with the AIMAll program.[33] Electrostatic Potential [ESP, $\varphi(r)$] and their extrema ($\varphi_{S,max}$ and $\varphi_{S,min}$), and electric field lines (EFLs) were calculated with the Multiwfn program.[34] Regions of non-covalent interactions were analyzed within the framework of the reduced density gradient (RDG).[35] The ESP was calculated and mapped on the RDG surface using the Multiwfn program.[34]

The electron charge redistribution was also analyzed with the Voronoi deformation density (VDD) analysis.[36] The Q_A atomic charges obtained with this method measure how much charge flows out ($Q_A > 0$) or into ($Q_A < 0$) the Voronoi cell of atom A upon interaction. The VDD charges were also computed with the Multiwfn program.[34]

Results and Discussion

Structures and Bond Strengths

In order to analyze only the interactions between the nitro groups without the influence of secondary interactions, all systems were optimized with the two molecular planes of the monomers perpendicular, and the oxygen atoms faced to each other (see Figure 1). In all complexes studied herein, imaginary frequencies were not observed. All structures along with their geometrical parameters are displayed in Figure 1. The average O···O distance (red values) decreases from F to I. However, the average N···O distance increases from F to Br and then it drops for I below the value of F. The O–N–O angle is reduced after complex formation (except for the complex with F). This geometrical change comes with the elongation of the N–O distances and the shortening of the X–N distances.

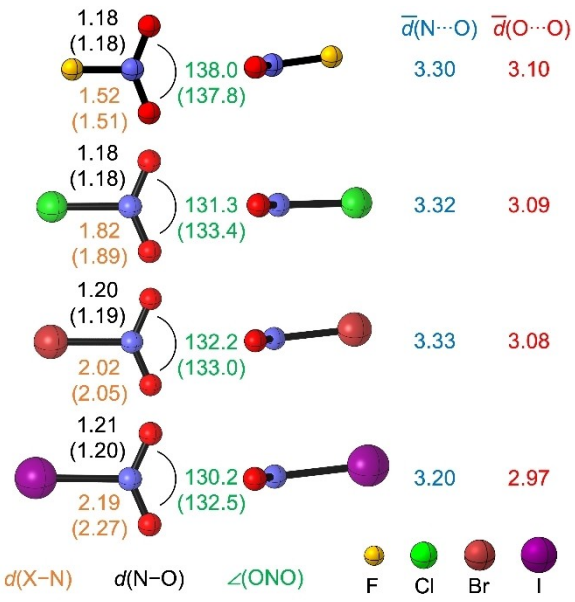

Figure 1. Equilibrium geometries (distances in Å and angles in degrees) of the $(XNO_2)_2$ dimers (X = F, Cl, Br, and I) computed at MP2/aug-cc-pVTZ. Values between parentheses correspond to monomers.

The $(XNO_2)_2$ complexes are very weakly stabilized. Table 1 collects the interaction energies computed at HF, MP2 and CCSD(T) levels of theory (interaction energies at the M06-2X level are collected in Table S1 in the Supporting Information). The interactions between nitryl halides are of stabilizing nature ($\Delta E_{int} < 0$) in the correlated methods used (see Table 1). These energies are in agreement with those reported for O···O interactions by Das et al.[12] for the formaldehyde dimer (−5.4 kJ mol^{-1}) and with the chalcogen bond $F_2O\cdots OH_2$ informed by Varadwaj (−5.6 kJ mol^{-1}).[15] The interaction energies computed at the MP2 level of theory show an increasing stabilization of the complexes from F to I. The CCSD(T) energies do not show a clear trend, however we can only say that the $(BrNO_2)_2$ and $(INO_2)_2$ complexes are slightly more stabilized than the $(FNO_2)_2$ and $(ClNO_2)_2$ dimers. Besides, a notable difference between the interaction energies at MP2/CCSD(T) and HF is observed for each complex. This difference clearly shows that correlation energy plays an important role in stabilizing these complexes. To test the effect of a non-electronegative substituent, we also included the $(HNO_2)_2$ dimer, but the optimization leads to another minimum structure with an O···N interaction.

The O···O distances are slightly higher than those reported by Varadwaj *et al.* for the following chalcogen bonds: $F_2O\cdots OH_2$ (2.809 Å)[15] and $F_2O\cdots OCH_2$ (2.788 Å), $F_2O\cdots FH$ (2.884 Å) and $F_2O\cdots OS$ (2.789 Å).[14] In the same sense Quiñonero et al. have carried out a theoretical study of nitryl halide heterodimers. They found that O···O distances are longer than the sum of the van der Walls (vdW) radii, so they were not catalogued as chalcogen interactions, but rather as vdW interactions.[37] However, this criterion is no longer recommended by the IUPAC.[38]

Energy Decomposition Analysis

Table 2 displays the LMOEDA values of the optimized dimers. From this data, one can notice that the exchange component covers around 44% of the attractive components, while the dispersion term represents about 35%. The electrostatic

Table 1. Interaction energies of $(XNO_2)_2$ (X = F, Cl, Br, I) dimers (in kJ mol^{-1}).

$(XNO_2)_2$	HF		MP2			CCSD(T)	
	[a]	[b]	[a]	[b]	[c]	[a]	[c]
$(FNO_2)_2$	4.3	4.8	−7.4	−6.4	−5.8	−7.2	−5.7
$(ClNO_2)_2$	8.6	9.2	−9.9	−8.6	−8.0	−7.9	−6.0
$(BrNO_2)_2$	7.0	14.1	−11.9	−10.3	−12.3	−9.6	−10.1
$(INO_2)_2$	13.7	14.3	−12.8	−12.5	−12.5	−8.9	−8.6

[a] aug-cc-pVTZ. [b] aug-cc-pVQZ. [c] Complete Basis Set (CBS) extrapolation scheme.

Table 2. Local molecular orbital energy decomposition (LMOEDA) analysis (in kJ mol^{-1}) of $(XNO_2)_2$ (X = H, F, Cl, Br, I) dimers obtained at MP2/aug-cc-pVTZ level of theory.

$(XNO_2)_2$	ΔE_{el}	ΔE_{ex}	ΔE_{rep}	ΔE_{pol}	ΔE_{disp}	ΔE_{int}
$(FNO_2)_2$	−5.6	−14.7	25.8	−1.3	−11.6	−7.4
$(ClNO_2)_2$	−10.1	−27.5	48.2	−2.0	−18.6	−9.8
$(BrNO_2)_2$	−6.6	−20.9	36.2	−1.7	−17.4	−10.4
$(INO_2)_2$	−8.9	−34.3	59.8	−2.9	−24.8	−11.1

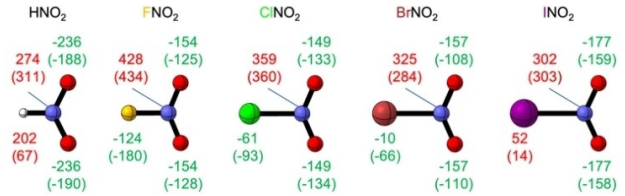

Figure 3. Voronoi deformation density charges in milli-electrons of XNO_2 (X = H, F, Cl, Br, I) molecules. Values in parenthesis correspond to the systems after complex formation.

forces play a smaller role in stabilizing these complexes, representing an average of 17% of the attractive components, while the polarization/orbital interactions can be neglected.

Since these energy components are distance dependent, to rationalize the trends, we computed the interaction energy profiles for the $(XNO_2)_2$ (X = H, F, Cl, Br, I) dimers as a function of the N···N interatomic distance. A non-relaxed potential energy surface scan was performed over the N···N distance and keeping the O–N···N–O dihedral angle fixed at 90 degrees. Then we decomposed the ΔE_{int}(LMOEDA) value in every step into the energy terms that contribute to the interaction energy. The results are plotted in Figure 2 (see complete dataset in Tables S2a–f).

The iodine-substituted dimer shows the strongest pair interaction energy along all the scanned distance, followed by $(BrNO_2)_2 > (ClNO_2)_2 > (FNO_2)_2 > (HNO_2)_2$ dimers. The latter shows a positive interaction energy along all the scan distance, which is in line with the fact that it cannot form a stable complex in the gas phase in this conformation. When going from F to I and then to H, a clear trend is seen. For instance, the systems with Cl and Br have a more stabilizing electrostatic component. The other halogen lines tend toward that of H.

To deepen our understanding of the electrostatic interactions we computed the VDD charges over all atoms before and after complex formation, and the values are displayed in Figure 3. It can be seen in this figure that after complex formation all oxygen atoms become less negative, while the X atoms (H, F, Cl. Br and I) get more electronic charge. Since

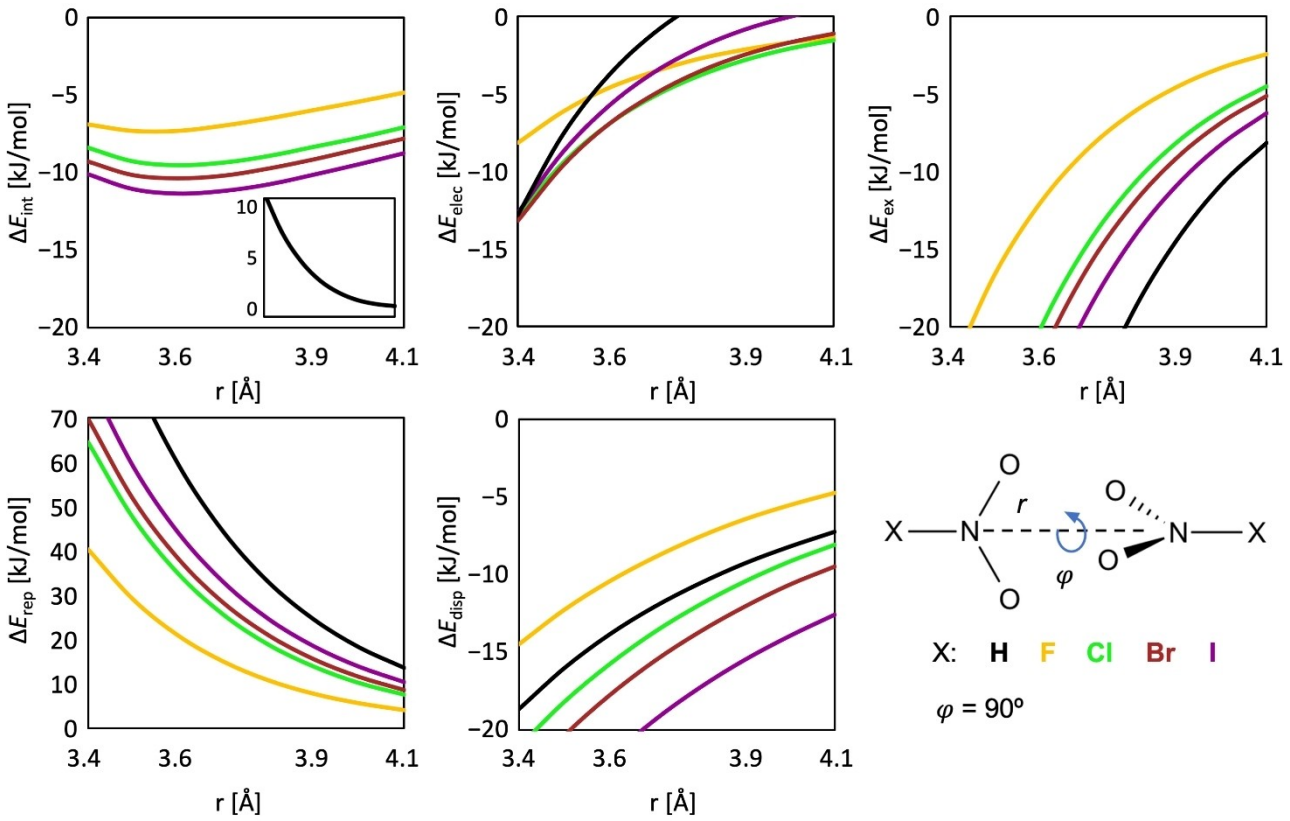

Figure 2. Decomposed energy terms [kJ mol^{-1}] as a function of the N···N distance r [Å] ($\varphi = 90°$) for $(XNO_2)_2$ (X = H, F, Cl, Br, I) dimers obtained at MP2/aug-cc-pVTZ level of theory.

E_{pol} is negligible (see Table 2), we cannot consider charge transfer interactions. Therefore, the VDD charges reflect an electronic charge shift from the O atoms to the X atoms due to the deformation experienced by their electron clouds.

Interestingly, the exchange energy is more negative for the $(HNO_2)_2$ dimer. Therefore, the interaction energy of the systems cannot be stabilized solely by the exchange component. Again, the other lines tend towards the black one, from F to I. Contrarily, the Pauli repulsion is larger for $(HNO_2)_2$ dimer, and for a specific distance, this component gradually decreases from I to F. Finally, the $(INO_2)_2$ dimer shows the most stabilizing dispersion energy along all the scanned distance, in line with its more stabilizing interaction energy.

Overall, both exchange and dispersion are the most important components. The $(HNO_2)_2$ dimer does not form a stable complex because of a large Pauli repulsion (ΔE_{rep}, see Figure 2) and low dispersion energy (ΔE_{disp}). As stated further up, at distances close to the equilibrium, both the exchange and the dispersion energies represent most of the attractive energy, each one reaching around 40 %.

On the other hand, the IQA scheme is a very useful tool to characterize the nature of the intermolecular interactions. Table 3 shows the deformation (E_{def}), classic (E_{cl}) and quantum (E_{xc}) contributions and interaction energies [E_i(IQA)].

In Table 3, the E_{int}(IQA) values do not show significant variations, they range from −8.8 to −11.3 kJ mol^{-1}. That is, there is a difference of only 2.5 kJ mol^{-1} between the most and least stable complexes, which is smaller than the normal uncertainty in the high-level of theory calculations. Table 3 also shows that in these dimers the quantum term (exchange and correlation), E_{xc}, is the dominant stabilizing component in each one of them. While the classic term, E_{cl}, is very low, negligible compared to E_{xc}.

The results of IQA analysis agree with those found by means of the LMOEDA method. In both global decomposition schemes, the classical term is negligible, and the components of exchange and correlation are the dominant ones.

In a study of hydrogen bonds within carboxylic acid dimers, Alkorta et al.[39] have shown that the contributions E_{def} and E_{xc} account of the electron density reorganization that takes place in the hydrogen-bonding region when the closed shells of the interacting molecules are in contact. The E_{def} term represents the repulsion of the closed shells and the concomitant removal of electron density from the bonding region. Even though the E_{xc} contribution is associated to the covalent character of the hydrogen bond, the exchange term E_x is the real term associated to the covalence degree between two atoms,[40] which is included within the exchange-correlation term E_{xc}. As can be seen in Table 3, $|E_{xc}| > E_{def}$ in all dimers, while for charged and neutral hydrogen-bonded complexes studied by Alkorta et al.[39] $|E_{xc}| < E_{def}$. Moreover, the IUPAC establishes that a covalent bond occurs when "a region of relatively high electron density between nuclei which arises at least partly from sharing of electrons and gives rise to an attractive force and characteristic internuclear distance".[41] In these complexes the intermolecular distances O···O are about 3.0 Å, while the bond distance in a single covalent bond O–O is about 1.5 Å (e.g. in hydrogen peroxide). In addition, there is no high electron density between nuclei of oxygen atoms (0.007 a.u.). Therefore, despite the large and negative exchange-correlation terms from the IQA scheme, we cannot say that O···O interactions have a certain covalent character.

So far, only global interaction energy decompositions have been performed. A more detailed analysis of the interatomic interactions involved follows. IQA method is a tool that allows the quantification of these interactions. Table 4 collects the classical (E_{cl}) and quantum (E_{xc}) contributions and interaction energies (E_{int}) of the intermolecular interatomic interactions O···O, O···N and N···N.

The total interaction between the nitro groups is attractive [E_{int}(O···O) + E_{int}(O···N) + E_{int}(N···N) < 0], where E_{int}-(O···N) is the only negative. Moreover, the E_{int}(O···O) > 0 and E_{cl}(O···O) also are positive. According to Pendás et al., this does not mean that the O···O interactions are repulsive.[42] In the words of Pendás himself "If we use interacting atoms the classical component contains the physical Coulombic interaction between subregions that are not directly related to the short-range domain which chemists associate with the chemical bond". In these complexes, two negatively charged oxygens are interacting in the dimer and are probably dominated by Coulombic repulsion between negative regions that are not in direction O···O interactions. Therefore, it is to be expected that in the O···O interatomic region, the electrostatic repulsion decreases, and the exchange-correlation predominates. Proof of this are the O···O bond paths (see

Table 3. Intermolecular IQA contributions (in kJ mol^{-1}) and total interaction energy at equilibrium geometries of $(XNO_2)_2$ (X = F, Cl, Br, I) dimers obtained at LSDA/aug-cc-pVTZ level of theory.

$(XNO_2)_2$	E_{def}	E_{cl}	E_{xc}	E_{int}(IQA)
$(FNO_2)_2$	47.4	−0.6	−55.8	−9.1
$(ClNO_2)_2$	64.7	−1.0	−75.0	−11.3
$(BrNO_2)_2$	52.2	−1.5	−60.7	−10.0
$(INO_2)_2$	74.0	−1.9	−80.9	−8.8

Table 4. IQA interatomic contribution (in au) in the O···O, O···N and N···N contacts.[a]

Dimer	interaction	E_{cl}(A,B)	E_{xc}(A,B)	E_{int}(A,B)
$(FNO_2)_2$	O···O	0.0716	−0.0173	0.0543
	O···N	−0.1980	−0.0030	−0.2010
	N···N	0.1360	−0.0001	0.1360
$(ClNO_2)_2$	O···O	0.0740	−0.0232	0.0508
	O···N	−0.1610	−0.0038	−0.1650
	N···N	0.0871	−0.0001	0.0870
$(BrNO_2)_2$	O···O	0.0817	−0.0191	0.0626
	O···N	−0.1535	−0.0027	−0.1560
	N···N	0.0715	−0.0001	0.0715
$(INO_2)_2$	O···O	0.0876	−0.0251	0.0619
	O···N	−0.1414	−0.0039	−0.1450
	N···N	0.0573	−0.0001	0.0572

[a] All magnitudes corresponding to O···O and O···N interactions were averaged.

Figure 4), which have been considered as channels of electronic exchange.[17] The values of the electrostatic interaction energy [$V_{en}(\mathbf{r}_b)$] between O···O interactions in all dimers are $V_{en}(\mathbf{r}_b) < 0$. This is because of the lowering of the potential energy in the interatomic region, caused by the accumulation of density that attracts the nuclei.

In Table 4 it can also be observed that O···N interactions play an important role in the stabilization of the complexes. Even more, the classical contribution of the O···N contact is greater than the sum of the exchange-correlation component in O···O, O···N and N···N, $[E_{cl}(O\cdots N) > E_{xc}(O\cdots O) + E_{xc}(O\cdots N) + E_{xc}(N\cdots N)]$.

It can be seen that the E_{cl}(O···N) term is affected by the electronegativity of the halogen atom. The more electronegative the atom, the stronger the electrostatic attraction between O and N atoms. Hence, although in the global EDA schemes (LMOEDA and IQA) the exchange and correlation components are the dominant ones (see Tables 2 and 3), we must not lose sight of the importance of O···N electrostatic interactions.

The ionization energy (IE) behaves in the opposite way to the Pauling electronegativity (χ). The lower this energy is, the more readily the atom/molecule becomes a cation. Moreover, as we already know, electronegativity will affect the electron cloud in the region opposite the N–X bonds. So, it is interesting to analyze how the IE and χ of the halogen atoms influence global and local interaction energies. Very good linear correlations have been found between IE and χ with the interatomic energies: E_{cl}(O···N), E_{cl}(N···N), E_{int}(O···N) and E_{int}(N···N) (R = 1 in all cases, see Figure S1 and S2). The important role played by the halogen atom as a substituent is evident. However, this is not so clear in the trends shown by the interaction energies in Tables 1 and 3. In this sense, it is observed very good correlations of χ and IE with ΔE_{int}-(LMOEDA) and ΔE_{int}(MP2) as shown in Figure S3, but not with ΔE_{int}(CBSs) and E_{int}(IQA). It appears that the interaction energies calculated with the MP2 method describe better the strength of these particular molecular interactions.

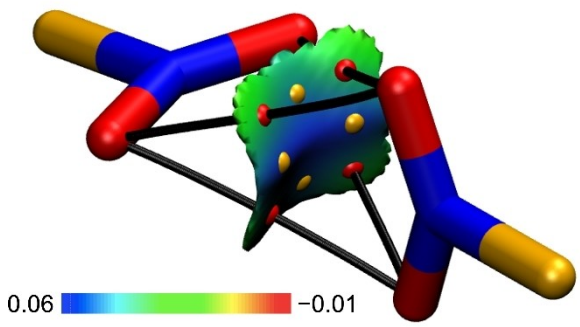

Figure 4. Molecular graph and gradient isosurface (RDG = 0.05) for $(FNO_2)_2$ dimer. The surfaces are colored on a blue-green-red scale, ranging 0.06 to −0.01 au. Blue indicates positive electrostatic potential and red shows negative electrostatic potential. Only positive values are observed. Red and yellow spheres indicate bond and ring critical points respectively.

According to Jabłoński et al., when the atoms are distant from each other (around 3.1 Å for O···O interactions), bond paths do not determine which interactions are dominants.[18] This idea is in line with our results. As shown in the IQA analysis of Table 4, the O···N interactions are the most important ones. However, the exchange-correlation component is greater in O···O interactions. This last observation is in accordance with the molecular graph shown in Figure 4 and with the concept of Pendas et al. They stablished that bond paths are privileged exchange-correlation channels.[17]

Topology of the Electron Density and Electrostatic Potential

Figure 4 shows the molecular graph of the $(FNO_2)_2$ dimer and the local topological properties at the O···O BCPs of all complexes are collected in Table 5. Topological parameters in these BCPs are typical of closed-shell interactions. According to Bader and Essén "these interactions are dominated by the contraction of charge away from the interatomic surface towards each of the nuclei".[43] The topological parameters do not show any significant trend among all the complexes. The electron density and Laplacian values at the BCPs are similar to those reported by Tsirelson *et al.* for the N_2O_4 crystal structure.[10] The delocalization indices [δ(O,O)] however, are much smaller than those reported for intramolecular O···O contacts (0.05–0.09 au).[4]

The topology of the ESP [$\varphi(\mathbf{r})$][44–46] has shown to be a reliable tool, especially to understand the role of electrostatic in molecular interactions.[47–50] The negative gradient of electrostatic potential, $-\nabla\varphi(\mathbf{r})$ [i.e. the electric field $E(\mathbf{r})$] indicates the direction of the Coulombic forces acting mainly on $\rho(\mathbf{r})$.[51] Figure 5 shows the EFLs of the $(FNO_2)_2$ dimer superimposed on the ESP map. When looking at the EFLs at the intermolecular region, some lines that come out from the local minima (red dots) of the topology of $\varphi(\mathbf{r})$ (lone pairs of the oxygen atoms) are headed toward the nucleus of the nitrogen atom.

Interestingly, one of the $\varphi(\mathbf{r})$ minima of each oxygen atom (the one closest to the other monomer) disappears in the complex. A similar situation has been observed in a study recently performed in the framework of the halogen bonds (XBs). In the equilibrium geometry of the O–Cl···B (B=CO, PH_3, SH_2, CS, NH_3, OH^-) complexes, the minimum of $\varphi(\mathbf{r})$ corresponding to the Lewis base disappears, and only positive electrostatic potentials are observed in the intermolecular region.[52]

Table 5. Average local topological properties (in au) at the O···O bond critical points for $(XNO_2)_2$ dimers (X = F, Cl, Br, I) obtained at LSDA/aug-cc-pVTZ level of theory.

$(XNO_2)_2$	$\rho(\mathbf{r}_b)$	$\nabla^2\rho(\mathbf{r}_b)$	$H(\mathbf{r}_b)$	δ(O,O)
$(FNO_2)_2$	0.0061	0.0229	0.0011	0.0611
$(ClNO_2)_2$	0.0079	0.0304	0.0015	0.0131
$(BrNO_2)_2$	0.0065	0.0233	0.0011	0.0502
$(INO_2)_2$	0.0082	0.0312	0.0015	0.0328

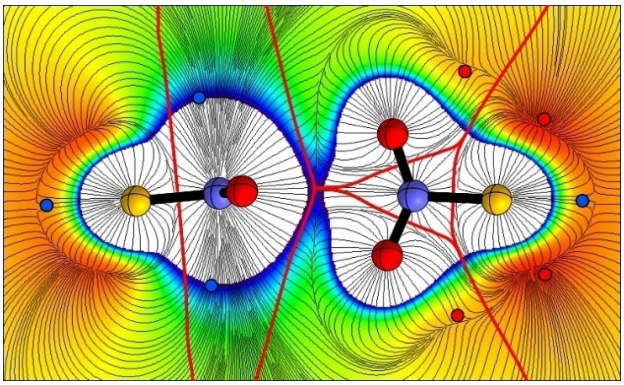

Figure 5. Electric field lines superimposed on the ESP map for $(FNO_2)_2$ dimer. Continuous red lines are interatomic surfaces (IAS). Local minima and maxima have been indicated with red and blue dots respectively. Color scale ranges from +167 (blue) to −42 kJ mol^{-1}.

According to the QTAIM the atomic basins are divided by interatomic surfaces (IAS), indicated by continuous-highlighted red lines in Figure 5. The topology of $\varphi(\mathbf{r})$ shows that there are regions of high electron density belonging to the oxygen atoms that feel the attraction of the nucleus of the nitrogen atom. These regions are defined as the electrostatic attraction region (EAR).[50] Due to the symmetry of the system, all the previous discussion is valid for the plane perpendicular to that in Figure 5, but in the opposite direction. In other words, the electronic cloud of oxygen atoms feels the attraction of the nucleus of the nitrogen atom of the other monomer and vice versa.

The maps generated from the RDG descriptor proposed by Johnson *et al.*[35] are also very useful for the study of molecular contacts and they represent another valuable topological tool. Figure 4 also shows the distributions of $\varphi(\mathbf{r})$ functions mapped on the isosurface of RDG = 0.5. As can be seen from this figure, the intermolecular region displays positive values of $\varphi(\mathbf{r})$. It can also be noticed that this observation is in line with recently published results on XBs. In these works, it was shown that in the bonding region of the XBs, the $\varphi(\mathbf{r})$ is always positive.[52–54] Even more, the more positive the potential in this region, the stronger the interaction. In Figure 5 it is also observed that in the central region the potential is more positive. So, the strongest interactions occur through this region. Moreover, the formation of this potential could be an indication of the formation of an electronic exchange channel.[52] The rest of the complexes have been tested, leading to the same results.

Overall, it is evident that from the analysis carried out in this section, the electrostatic interactions between oxygen atoms and nitrogen nuclei are important to stabilize the complexes.

Probing O···O Interactions in Other Nitrocompounds

In this section we further analyzed the presence of intermolecular O···O interactions within more realistic environments. For instance, tetranitromethane[55] (4NM, refcode ZZZWEW) is liquid at room temperature (m.p. 13–14 °C, b.p. 126 °C), and due to its molecular structure short contacts between oxygen atoms must be present. We therefore took this molecule as a model compound to explore the presence of intermolecular O···O interactions between nitro groups. In the last seven decades, the structure of this molecule has been one of the most controversial. According to Vishnevskiy et al. the identity of this highly symmetric molecule has been well established but its structure in different phases is not free of controversy. Despite the large number of studies carried out, there is still no consistent description. By applying a 4D dynamic model for the treatment of data obtained by gas-phase electron diffraction, these authors described the extremely dynamic behavior of 4NM in this phase.[55] They also state that "all quantum-chemical calculations predicted S_4 symmetry for the ground state and no other conformational minima. However, the four lowest vibrational frequencies (MP2/cc-pVTZ) are located at 57 (E, doubly degenerate), 64 (A), and 84 cm^{-1} (B), and all correspond to internal rotations of the nitro groups. The next higher energetic vibration is found at a significantly higher frequency of 174 cm^{-1}". So, it appears that in the gas-phase the 4 nitro groups rotate freely around the C–N bonds.

The study of the torsional movement of the nitro groups in the dimer of 4NM is not computationally easy to make, due to the complicated correlation of these movements, which depend on each other. To go deeper into this question, we have made a rigid scan in the $(FNO_2)_2$ dimer, varying the dihedral angle O–N···N–O and keeping constant the O···O distances and the rest of the geometric parameters. At each point of the scan, we have performed energetic decompositions using the LMOEDA and IQA schemes, and the results are shown in Figure S4. In both methods it is observed that the rotational barrier is relatively low (around 3–5 kJ mol^{-1}), so it is expected that at room temperature or higher, the nitro groups rotate freely. Besides, it is clearly visible that the exchange and dispersion terms (ΔE_{ex} and ΔE_{disp} in LMOEDA and E_{xc} in IQA) are always negative throughout the rotation range ($0 \leq \varphi \leq 180°$), being more pronounced at the equilibrium geometry ($\varphi = 90°$) counteracted by a larger repulsion, while the electrostatic component takes relatively small negative values in the equilibrium position. In other words, electronic exchange and correlation are the components responsible for the dimer remaining attached while the nitro groups rotate.

We also considered two related compounds: Trinitromethane[56] (3NM, b.p. 175.1 °C, refcode HEVRUV) and chlorotrinitromethane[57] (Cl3NM, b.p. 124.6, refcode RUBSUD). For the sake of comparison, we analyzed two types of dimers. First, we took a dimer from their crystal structures (*a* dimers) and then we created artificial dimers by placing the –H, –NO_2, and –Cl groups away from each other (*b* dimers).

All these dimers were then fully optimized, and their structure and molecular graphs are shown in Figure 6.

As can be seen in Figure 6a, all the dimers show at least one intermolecular BCP between N and O atoms. This is an interaction between oxygen lone pairs and the N π-hole. All local topological properties are collected in Tables S3a–c. The $(3NM)_2$-*a* dimer shows a stable C–H···O hydrogen bond and two N···O interactions. There is also a BCP between the central C and an O atom with a high ellipticity value (3.3409 au) that indicates a rather unstable interaction. Moving to $(4NM)_2$, the conformer -*a*- shows BCP between N and O, however it also shows high instability due to a large ellipticity value (5.2258 au). Therefore, both conformers are interacting by pure O···O contacts. With regards to the

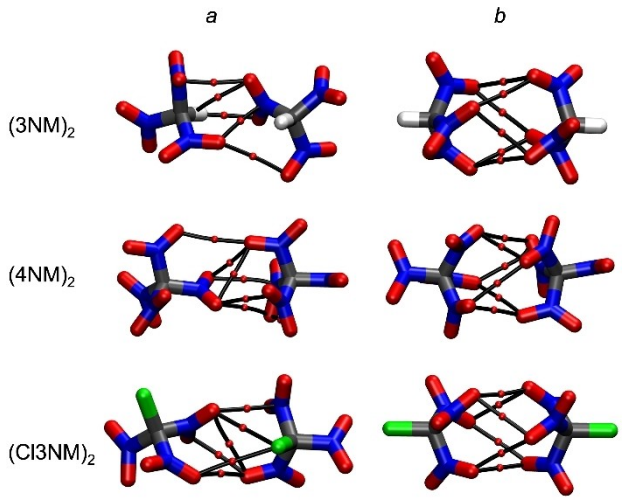

Figure 6. Molecular structures and graphs of two conformations (*a* and *b*) of tetranitromethane $(4NM)_2$, trinitromethane $(3NM)_2$ and chlorotrinitromethane $(Cl3NM)_2$ dimers.

Table 6. Local molecular orbital energy decomposition (LMOEDA) analysis computed at MP2/6-311++G(2d,2p)//M062X/6-311++G(2d,2p) level of theory (in kJ mol^{-1}).

Dimer	ΔE_{el}	ΔE_{ex}	ΔE_{rep}	ΔE_{pol}	ΔE_{disp}	ΔE_{int}
$(3NM)_2$-*a*	−31.8	−51.2	93.5	−16.7	−29.7	−36.0
$(3NM)_2$-*b*	−7.7	−31.5	56.3	−9.7	−37.3	−29.8
$(4NM)_2$-*a*	−20.1	−46.2	83.9	−12.3	−41.8	−36.6
$(4NM)_2$-*b*	−16.6	−53.7	97.0	−15.7	−55.5	−44.5
$(Cl3NM)_2$-*a*	−17.2	−41.9	74.5	−10.0	−36.3	−30.9
$(Cl3NM)_2$-*b*	−7.7	−34.5	61.4	−9.9	−42.0	−32.7

Table 7. Intermolecular IQA contributions (in kJ mol^{-1}).and total interaction energy at equilibrium geometries of $[XC(NO_2)_3]_2$ (X = H, Cl, and NO_2) dimers obtained at LSDA/6-311++G(2d,2p)//M062X/6-311++G(2d,2p) level of theory.

Dimer	E_{def}	E_{cl}	E_{xc}	E_{int}
$(3NM)_2$-*a*	135.5	−19.1	−150.8	−34.4
$(3NM)_2$-*b*	111.4	0.0	−130.0	−18.6
$(4NM)_2$-*a*	133.4	−7.8	−147.6	−22.0
$(4NM)_2$-*b*	157.7	−5.6	−183.2	−31.0
$(Cl3NM)_2$-*a*	117.3	−6.5	−133.8	−23.0
$(Cl3NM)_2$-*b*	111.7	−0.2	−129.1	−17.6

$(Cl3NM)_2$-*a* dimer, there are two stable BCP between O and Cl atoms that are not related to classical σ-hole halogen bonds, in line with the experimental results of Politzer et al.[55] They found out that the entire surface of chlorine is rather positive. Besides, -*b*- type dimers (See Figure 6) show only BCPs between O atoms, and their graph patterns are almost equal. All these O···O contacts share the same characteristics as those found in nitryl halides.

Table 6 and 7 display the EDA analysis within the LMOEDA and IQA schemes respectively (Interaction energies computed at the M062X level are collected in Table S4). The energy separation between both conformers is very shallow and below 8 kJ mol^{-1} (2 kcal mol^{-1}). These energies are also comparable to that of the water dimer[58] (around 20 kJ mol^{-1}). Both methods agree with the fact that the electrostatic (or classical) interaction is less dominant within *b* type dimers, and this contributes little to their stabilization.

LMOEDA method show that the exchange component covers around 38% of the attractive components, while the dispersion term represents about 37%. The electrostatic forces play a smaller role in stabilizing these complexes, representing an average of 14% of the attractive components. However, a particular case in the $3NM_2$-*a* dimer is observed. The electrostatic component is similar to dispersion term, this is probably due to the fact that there are two C–H···O hydrogen bonds (see Figure 5b) in this complex that cause an increase in the electrostatic component.

The analysis of the IQA data shows similar results to those found for nitryl halides dimers. In Table 7 is observed that in these dimers the term E_{xc} is the dominant stabilizing component in each one of them. While the E_{cl} is very low, negligible compared to E_{xc}.

The results shown by LMOEDA and IQA are consistent with those found for nitryl halides dimers.

Conclusions

In this contribution we have shown how the joint analysis of different EDAs and the topology of the electron density, the electrostatic potential and its derivatives functions is able to unequivocally explain the unusual interactions between oxygen atoms of nitro groups.

In these interactions, the global interaction energy decompositions LMOEDA and IQA indicate that the Coulombic interaction is negligible, and the components of exchange and correlation are the dominant ones. The LMOEDA scheme indicates that exchange and dispersion contribute almost equally to the attractive part of the interaction energy. These components are also more stabilizing for those with iodine, follow by Br > Cl > F. Besides, while the $(HNO_2)_2$ dimer has the strongest exchange energy, it displays a low dispersion energy, therefore, this attractive component is the key leading factor.

A detailed analysis of the interatomic interactions through local IQA shows that O···O bond paths are sensing the exchange-correlation energy, a factor of importance for

the stabilization of the complexes. This was also revealed by the non-local energy decomposition analysis. Besides, the local IQA analysis in conjunction with EFLs and RDG show that O···N electrostatic interactions are also important for stabilizing the complexes established between nitro groups. These interactions are affected by the electronegativity of the halogen atom: the more electronegative the atom, the stronger the electrostatic attraction between O and N atoms.

Finally, we have shown that the interactions between nitro compounds like tetranitromethane and some derivatives are governed by the same principles as those observed within our simpler models. Exchange and dispersion are the dominant components that keep the compounds bounded during the rotation of the nitro groups.

We think this work demonstrates the importance of a joint study of EDAs and the topology of real physical observables.

Acknowledgements

We thank to General Secretariat of Science and Technology (SGCyT) of the National University of the Northeast (UNNE), and Secretariat of Science and Technology (SECyT) of the National Technological University – Regional Faculty of Resistencia (UTN – FRRe) for financial support. The authors also thank the National Scientific and Technical Research Council (CONICET) of Argentina for research positions.

Conflict of Interest

The authors declare no conflict of interest.

Data Availability Statement

The data that support the findings of this study are available from the corresponding author upon reasonable request.

Keywords: electrostatic interactions · exchange interactions · noncovalent interactions · EDA · QTAIM

[1] J. Cioslowski, S. T. Mixon, E. D. Fleischmann, *J. Am. Chem. Soc.* **1991**, *113*, 4751–4755.
[2] R. F. W. Bader, *Atoms in Molecules: A Quantum Theory*, Clarendon Press, Oxford, **1994**.
[3] E. A. Zhurova, V. G. Tsirelson, A. I. Stash, A. A. Pinkerton, *J. Am. Chem. Soc.* **2002**, *124*, 4574–4575.
[4] A. H. Pakiari, K. Eskandari, *J. Mol. Struct.: THEOCHEM* **2007**, *806*, 1–7.
[5] M. Jabłoński, *J. Phys. Chem. A* **2012**, *116*, 3753–3764.
[6] C. Sharma, A. K. Singh, J. Joy, E. D. Jemmis, S. K. Awasthi, *RSC Adv.* **2016**, *6*, 91689–91693.
[7] T. Fellowes, B. L. Harris, J. M. White, *Chem. Commun.* **2020**, *56*, 3313–3316.
[8] R. Bianchi, G. Gervasio, D. Marabello, *Inorg. Chem.* **2000**, *39*, 2360–2366.
[9] T. Arumuganathan, A. Srinivasa Rao, S. K. Das, *J. Chem. Sci.* **2008**, *120*, 297–304.
[10] V. G. Tsirelson, A. V. Shishkina, A. I. Stash, S. Parsons, *Acta Crystallogr. Sect. B* **2009**, *65*, 647–658.
[11] M. V. Vener, A. N. Egorova, V. G. Tsirelson, *Chem. Phys. Lett.* **2010**, *500*, 272–276.
[12] M. Das, B. N. Ghosh, A. Bauzá, K. Rissanen, A. Frontera, S. Chattopadhyay, *RSC Adv.* **2015**, *5*, 73028–73039.
[13] Y. Liu, T. Yu, W. Lai, Y. Ma, Z. Ge, F. L. Yang, P. Y. Liang, Y. Long, P. P. Zhou, Z. Yang, *New J. Chem.* **2021**, *45*, 6136–6143.
[14] P. R. Varadwaj, A. Varadwaj, H. M. Marques, P. J. MacDougall, *Phys. Chem. Chem. Phys.* **2019**, *21*, 19969–19986.
[15] P. R. Varadwaj, *Molecules* **2019**, *24*, 3166.
[16] M. A. A. Ibrahim, E. M. Z. Telb, *ACS Omega* **2020**, *5*, 21631–21640.
[17] A. M. Pendás, E. Francisco, M. A. Blanco, C. Gatti, *Chem. Eur. J.* **2007**, *13*, 9362–9371.
[18] M. Jabłoński, *ChemistryOpen* **2019**, *8*, 497–507.
[19] E. O. Levina, M. G. Khrenova, V. G. Tsirelson, *J. Comput. Chem.* **2021**, *42*, 870–882.
[20] *Gaussian 09 (Revision D.01)*, M. J. Frisch, G. W. Trucks, H. B. Schlegel, G. E. Scuseria, M. A. Robb, J. R. Cheeseman, G. Scalmani, V. Barone, B. Mennucci, G. A. Petersson, H. Nakatsuji, M. Caricato, X. Li, H. P. Hratchian, A. F. Izmaylov, J. Bloino, G. Zheng, J. L. Sonnenberg, M. Hada, M. Ehara, K. Toyota, R. Fukuda, J. Hasegawa, M. Ishida, T. Nakajima, Y. Honda, O. Kitao, H. Nakai, T. Vreven, J. A. Montgomery, Jr., J. E. Peralta, F. Ogliaro, M. Bearpark, J. J. Heyd, E. Brothers, K. N. Kudin, V. N. Staroverov, T. Keith, R. Kobayashi, J. Normand, K. Raghavachari, A. Rendell, J. C. Burant, S. S. Iyengar, J. Tomasi, M. Cossi, N. Rega, J. M. Millam, M. Klene, J. E. Knox, J. B. Cross, V. Bakken, C. Adamo, J. Jaramillo, R. Gomperts, R. E. Stratmann, O. Yazyev, A. J. Austin, R. Cammi, C. Pomelli, J. W. Ochterski, R. L. Martin, K. Morokuma, V. G. Zakrzewski, G. A. Voth, P. Salvador, J. J. Dannenberg, S. Dapprich, A. D. Daniels, O. Farkas, J. B. Foresman, J. V. Ortiz, J. Cioslowski, D. J. Fox, Gaussian, Inc., Wallingford CT, **2013**.
[21] C. Møller, M. S. Plesset, *Phys. Rev.* **1934**, *46*, 618–622.
[22] B. P. Pritchard, D. Altarawy, B. Didier, T. D. Gibson, T. L. Windus, *J. Chem. Inf. Model.* **2019**, *59*, 4814–4820.
[23] A. Halkier, T. Helgaker, P. Jørgensen, W. Klopper, J. Olsen, *Chem. Phys. Lett.* **1999**, *302*, 437–446.
[24] A. Halkier, W. Klopper, T. Helgaker, P. Jørgensen, P. R. Taylor, *J. Chem. Phys.* **1999**, *111*, 9157–9167.
[25] P. Jurecka, J. Sponer, J. Cerný, P. Hobza, *Phys. Chem. Chem. Phys.* **2006**, *8*, 1985–1993.
[26] a) L. M. Mentel, E. J. Baerends, *J. Chem. Theory Comput.* **2014**, *10*, 252–267; b) I. Alkorta, J. Elguero, S. J. Grabowski, *Phys. Chem. Chem. Phys.* **2015**, *17*, 3261–3272; c) D. J. R. Duarte, N. M. Peruchena, I. Alkorta, *J. Phys. Chem. A* **2015**, *119*, 3746–3752.
[27] P. Politzer, K. E. Riley, F. A. Bulat, J. S. Murray, *Comput. Theor. Chem.* **2012**, *998*, 2–8.
[28] M. J. S. Phipps, T. Fox, C. S. Tautermann, C.-K. Skylaris, *Chem. Soc. Rev.* **2015**, *44*, 3177–3211.
[29] P. Su, H. Li, *J. Chem. Phys.* **2009**, *131*, 014102.
[30] K. Morokuma, K. Kitaura in *Chemical Applications of Atomic and Molecular Electrostatic Potentials* (Eds. P. Politzer, D. G. Truhlar) Springer, Boston, MA, **1981**, pp. 215–242.
[31] M. A. Blanco, A. Martín Pendás, E. Francisco, *J. Chem. Theory Comput.* **2005**, *1*, 1096–1109.
[32] M. W. Schmidt, K. K. Baldridge, J. A. Boatz, S. T. Elbert, M. S. Gordon, J. H. Jensen, S. Koseki, N. Matsunaga, K. A. Nguyen, S. Su, T. L. Windus, M. Dupuis, J. A. J. Montgomery, *J. Comput. Chem.* **1993**, *14*, 1347–1363.
[33] T. A. Keith, *AIMAll (Version 11.12.19)*, TK Gristmill Software, Overland Park KS; aim.tkgristmill.com.
[34] T. Lu, F. Chen, *J. Comb. Chem.* **2012**, *33*, 580–592.
[35] E. R. Johnson, S. Keinan, P. Mori-Sánchez, J. Contreras-García, A. J. Cohen, W. Yang, *J. Am. Chem. Soc.* **2010**, *132*, 6498–6506.
[36] C. Fonseca Guerra, J.-W. Handgraaf, E. J. Baerends, F. M. Bickelhaupt, *J. Comput. Chem.* **2003**, *25*, 189–210.
[37] D. Quiñonero, A. Bauzá, G. Sánchez-Sanz, C. Trujillo, I. Alkorta, J. Elguero, *New J. Chem.* **2016**, *40*, 9060–9072.
[38] E. Arunan, G. R. Desiraju, R. A. Klein, J. Sadlej, S. Scheiner, I. Alkorta, D. C. Clary, R. H. Crabtree, J. J. Dannenberg, P. Hobza, H. G. Kjaergaard, A. C. Legon, B. Mennucci, D. J. Nesbitt, *Pure Appl. Chem.* **2011**, *83*, 1619–1636.
[39] I. Alkorta, I. Mata, E. Molins, E. Espinosa, *Chem. Eur. J.* **2016**, *22*, 9226–9234.
[40] A. F. Silva, L. J. Duarte, P. L. A. Popelier, *Struct. Chem.* **2020**, *31*, 507–519.
[41] *IUPAC. Compendium of Chemical Terminology*, 2nd ed. (Eds. A. D. McNaught, A. Wilkinson), Blackwell Scientific Publications, Oxford, **1997**.

[42] A. M. Pendás, J. L. Casals-Sainz, E. Francisco, *Chem. Eur. J.* **2019**, *25*, 309–314.
[43] R. F. W. Bader, H. Essén, *J. Chem. Phys.* **1984**, *80*, 1943–1960.
[44] A. A. Baskakov, A. A. Varnek, V. G. Tsirelson, R. P. Ozerov, *J. Struct. Chem.* **1985**, *25*, 636–637.
[45] S. R. Gadre, S. A. Kulkarni, I. H. Shrivastava, *J. Chem. Phys.* **1992**, *96*, 5253–5260.
[46] C. Bureau, M. Defranceschi, J. Delhalle, G. Lécayon, D. R. Salahub, *J. Mol. Struct.: THEOCHEM* **1995**, *330*, 279–285.
[47] I. Mata, E. Molins, I. Alkorta, E. Espinosa, *J. Phys. Chem. A* **2007**, *111*, 6425–6433.
[48] I. Mata, I. Alkorta, E. Molins, E. Espinosa, *ChemPhysChem* **2012**, *13*, 1421–1424.
[49] I. Mata, I. Alkorta, E. Molins, E. Espinosa, *Chem. Phys. Lett.* **2013**, *555*, 106–109.
[50] I. Mata, E. Molins, I. Alkorta, E. Espinosa, *J. Phys. Chem. A* **2015**, *119*, 183–194.
[51] N. Bouhmaida, M. Dutheil, N. E. Ghermani, P. Becker, *J. Chem. Phys.* **2002**, *116*, 6196–6204.
[52] M. O. Miranda, D. J. R. Duarte, *ChemistrySelect* **2021**, *6*, 680–684.
[53] D. J. R. Duarte, G. J. Buralli, N. M. Peruchena, *Chem. Phys. Lett.* **2018**, *710*, 113–117.
[54] E. Bartashevich, V. Tsirelson, *J. Comput. Chem.* **2017**, *39*, 573–580.
[55] Y. V. Vishnevskiy, D. S. Tikhonov, J. Schwabedissen, H. G. Stammler, R. Moll, B. Krumm, T. M. Klapötke, N. W. Mitzel, *Angew. Chem. Int. Ed.* **2017**, *56*, 9619–9623; *Angew. Chem.* **2017**, *129*, 9748–9752.
[56] H. Schödel, R. Dienelt, H. Bock, *Acta Crystallogr., Sect. C: Cryst. Struct. Commun.* **1994**, *50*, 1790–1792.
[57] M. Göbel, B. H. Tchitchanov, J. S. Murray, P. Politzer, T. M. Klapötke, *Nat. Chem.* **2009**, *1*, 229–235.
[58] M. W. Feyereisen, D. Feller, D. . Dixon, *J. Phys. Chem.* **1996**, *100*, 2993–2997.

Manuscript received: October 14, 2022
Revised manuscript received: December 6, 2022
Accepted manuscript online: December 14, 2022
Version of record online: January 4, 2023